



STScI | SPACE TELESCOPE
SCIENCE INSTITUTE

When there is a discrepancy between the information in this technical report and information in JDox, assume JDox is correct.

JWST TECHNICAL REPORT

Title: Analysis of NIRISS SOSS Photometric Calibration Observations From Commissioning Through Cycle 3	Doc #: JWST-STScI-009248, SM-12 Date: 24 November 2025 Rev: -
Authors: Kevin Volk Phone: 4409	Release Date: 5 January 2026

1 Abstract

The photometric calibration factors for the NIRISS Single Object Slitless Spectroscopy mode have been re-determined using the absolute calibration observations from commissioning through cycle 3. Observations have been obtained for one white dwarf star, two A-type stars, and two solar-like stars. The observations of the A0V standard BD+60°1753 from the stability monitoring programs have also been analyzed. For each observation the zodiacal light and telescope background has been removed from the exposures before the spectral extraction, which was not done when the initial photometric calibration was carried out in commissioning. Currently the JWST data reduction pipeline extracts only orders 1 and 2 so these orders were recalibrated, while order 3 which was calibrated in commissioning was not recalibrated here. For order 1 there is a reduction in the photometric calibration values by between 2% and 8% with respect to the values derived in commissioning from the short wavelengths to the long wavelengths. For order 2 the changes are larger, up to 15% in some cases, and have larger uncertainties. The values are particularly uncertain at wavelengths greater than 1 μm where the spectral signal becomes low. Different results are obtained depending on whether the measurements are assumed to have purely statistical uncertainties or whether they are assumed to differ due to systematic effects. There is some indication in the measurements that the solar-like standards give a slightly different result than is obtained from the hotter stars. The new photometric values are estimated to be accurate to within $\pm 1\text{-}2\%$ over the spectral range where there is significant signal, for wavelengths from 0.63 to 0.94 μm in order 2 and all of order 1.

2 Introduction

The NIRISS Single Object Slitless Spectroscopy (SOSS) mode allows slitless spectroscopy of stars over the wavelength range 0.6 to 2.85 μm primarily for time series observations such as exoplanet transit science. The spectra produced in this mode are defocused using a cylindrical lens attached to the GR700XD grism, producing a relatively wide point-spread function (PSF) with a typical full width at half maximum of 23 pixels. The SOSS mode and the results from NIRISS commissioning are described in Albert et al. (2023).

Operated by the Association of Universities for Research in Astronomy, Inc., for the National Aeronautics and Space Administration under Contract NAS5-03127

Check with the JWST SOCCER Database at: <https://soccer.stsci.edu>

To verify that this is the current version.

The initial calibration of the mode in commissioning used observations of a single photometric standard, BD+60°1753, in program 1091. The commissioning photometric calibration is described in Volk and the NIRISS Team (2022). The calibration was carried out using a single spectral extraction of orders 1, 2, and 3 which did not correct for either the sky background signal or the order overlap. The extraction used a ± 20 -pixel box around the center of the trace as determined from the observations. The JWST pipeline extraction for this mode using the ATOCA algorithm (Darveau-Bernier et al., 2022) was not fully functional at the time the reductions were carried out. The code extracted part of the traces, but without any deblending (which the algorithm was intended to provide). It was known that this calibration would need to be revised later to correct for these effects, but at the time there was insufficient knowledge of the properties of the mode to allow a better calibration. The photometric calibration was also derived without an aperture correction, since the JWST data reduction pipeline extracts the spectra from a fixed aperture that should be the same for the photometric standard star and for all science observations.

Volk (2024) describes analysis of the cycle 1 photometric calibration measurements in programs 1536, 1537, and 1538. The ATOCA algorithm in the pipeline was fully operational when this analysis was done which allowed deblending of orders 1 and 2 in this analysis. These observations of the photometric standards G191-B2B, GSPC P177-D, and 2MASS J17430448+6655015, which are fainter than BD+60°1753, showed significant effects from the sky background which were not obvious in the commissioning observations of BD+60°1753. Although an attempt was made to subtract out the background signal using a background template derived from the commissioning observations, the results still showed a residual background component. Nonetheless, a revision was made to the SOSS photometric calibration values based on this work.

This report discusses analysis of the photometric calibration observations from commissioning through the end of cycle 3. Along with the availability of more observations, there have been significant improvements in the background subtraction for SOSS mode. There are also some improvements in other aspects of the JWST data reduction pipeline that have taken place between the previous analysis in 2024 and the current analysis, the most notable being the addition of the `pixel_replace` step to interpolate over bad pixels in the spectral trace and some changes in the handling of large cosmic ray events in the data reduction.

3 The Observations

The current analysis uses all SOSS mode observations of photometric standard stars from NIRISS commissioning through the end of cycle 3. This includes the photometric calibration programs 1091, 1536, 1537, 1538, 4448, and 6607 plus the photometric stability observations in programs 1539, 4448, and 6608. A total of 25 stability observations and 6 “regular” photometric observations are included. The list of individual observations is given in Table 3 in the Appendix. Some of the observations include a short exposure in the F277W+GR700XD configuration; exposures in that configuration are not analyzed here because the JWST data reduction pipeline does not currently extract such spectra. For this analysis all the raw “uncal” files for these observations were processed in the JWST

data reduction pipeline version 1.18.0 (Bushouse et al. 2025) in CRDS context `jwst_1364.pmap` (CRDS version 12.1.5). The initial `calwebb_detector1` stage of the pipeline was run on all files. Before proceeding to the `calwebb_spec2` pipeline for the spectral extraction each rate file was background subtracted as is described below. Once the background subtraction was done, the `calwebb_spec2` part of the pipeline was run to extract the spectra of the individual exposures. At this stage the `pixel_replace` step was turned on for the observations, to interpolate values for bad pixels in the two-dimensional spectral images. That step is normally off for the NIRISS spectral modes, and it would not normally be used for SOSS science observations because it is likely to introduce correlated noise into the individual spectra. While that is a concern for exoplanet transit observations, it is not for the photometric calibration observations. In this version of the JWST pipeline only spectral orders 1 and 2 are extracted. In some of the previous versions of the pipeline order 3 would also have been extracted, and it is intended that this functionality will be available in future pipeline builds; for the current analysis, the order 3 spectra were not extracted for analysis because it was intended that all the steps except for the background subtraction would be done in the JWST pipeline. The background subtraction is due to be added to the pipeline in the fall 2025 release. The order 3 spectral extraction will also be put back into the pipeline either in the upcoming release or the next release after that, at which point it will be necessary to redetermine the order 3 photometric calibration.

Once the spectra were extracted, the individual spectra for each integration and order were subject to sigma-clipped averaging using the `astropy sigma_clipped_stats` routine with a clipping threshold of 3.0σ and up to 5 iterations. The mean spectra so produced had units of MJy based on the current photometric calibration of the SOSS mode in the pipeline, which was derived from the work reported in Volk (2024). Taking a ratio of the observed spectra in orders 1 and 2 to the interpolated stellar model template for the photometric standard star produces a ratio value as a function of wavelength that brings the measured spectrum into agreement with the assumed standard star spectrum.

4 Background Subtraction

All NIRISS SOSS observations have a sky plus telescope background component that is produced primarily by the zodiacal light spectrum of dust particles in the solar system. This emission fills the NIRISS pick-off mirror field of view, so it is dispersed by the GR700XD grism onto the detector. The original expectation was that this background would have a fixed shape and simply scale up or down depending on the sky pointing. The prediction is that the telescope background is small compared to the zodiacal emission at the wavelengths covered by the SOSS mode. The observed order 1 spectrum is limited to wavelengths less than $\approx 2.85 \mu\text{m}$ by the detector, but it extends to wavelengths beyond $5 \mu\text{m}$ at which point the detector long wavelength cut-off is reached. The same is true for the other orders, although we do not have good observations of the longer wavelength response on-sky.

A background template image was derived from commissioning observations in program 1092 observation 1, where full frame images were taken with the GR700XD grism with the target first at the normal acquisition position and then offset down to the middle of the detector. The images show a discontinuity in the background signal at approximately column 705. This is

due to a change in the orders that contribute to the background signal; to the right of the break, orders 0 to 4 contribute to the background signal (as well as order -1 just at the right edge of the subarray), while to the left of the break order 0 no longer contributes. The two full frame images were combined with manual masking of the source spectra to produce a background template image. The individual rows of the output image were then fit with low order polynomials in two sections to reduce the noise, producing the background template image shown in Figure 1. As the discontinuity is tilted with respect to the detector columns, the fitting which was done on a fixed range of columns on each side does not cover the full detector. A line has been introduced into the image at the lower edge of the SUBSTRIP256 sub-array that is used for the photometric calibration observations discussed here as well as most of the science observations.

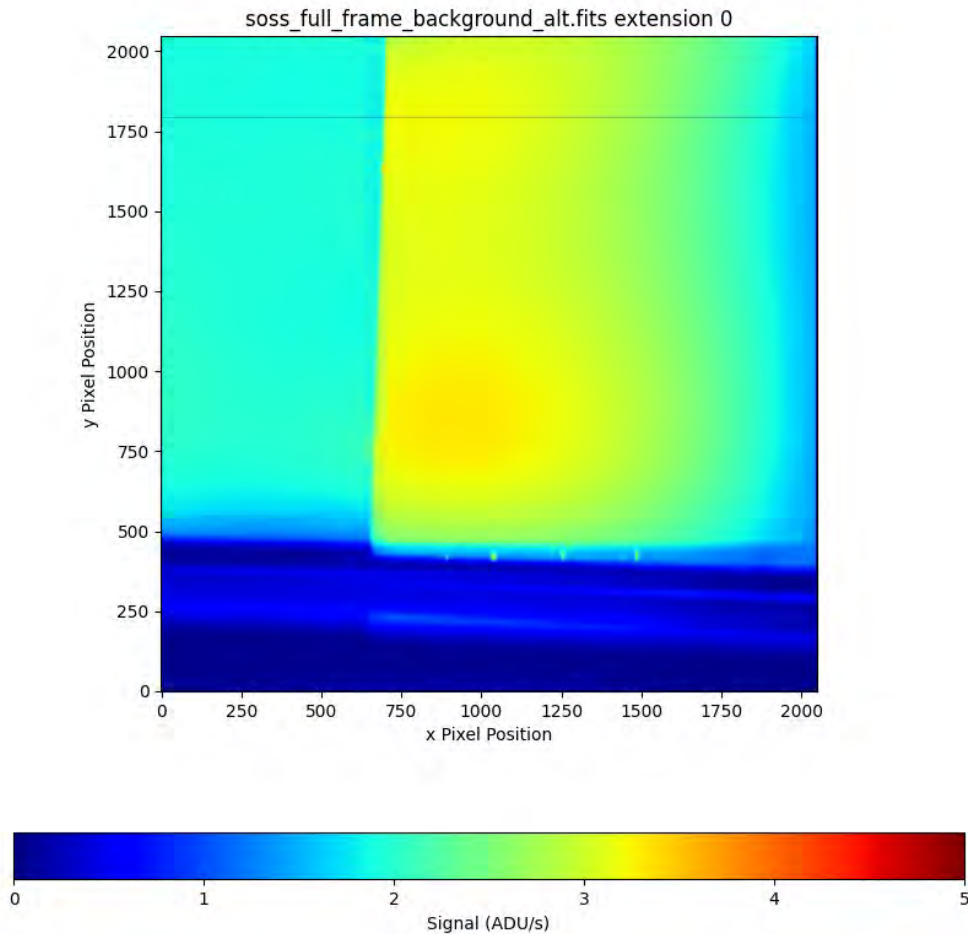


Figure 1: The SOSS mode full frame background template image. A line has been drawn across the image at the lower edge of the SOSS SUBSTRIP256 image area used for regular SOSS mode science and calibration observations.

Check with the JWST SOCCER Database at: <https://soccer.stsci.edu>
To verify that this is the current version.

Although the template was made in commissioning, it was not applied in the original reduction of the commissioning photometric calibration of SOSS mode. The discontinuity in the background did not show up in the extracted count-rate spectra of BD+60°1753 at the expected wavelength of about 2.14 μm . At that time, the NIRSS team lacked suitable algorithms for carrying out the background subtraction and it was assumed that if the discontinuity was not seen in the extracted spectrum that the effect would be small.

For the subsequent cycle 1 photometric observations of the fainter standard stars there was an obvious discontinuity in the order 1 spectra at around 2.14 μm in order 1, and in some cases also in orders 2 and 3 at wavelengths corresponding to the background break. However, the initial attempts to remove the background were not successful because it was difficult to properly estimate the scaling needed and because the background shape was changing between the different observations.

Due to the discovery that the background shape was not as stable as had been expected before launch, calibration programs were undertaken to measure the background at various sky positions to probe the dependence of the background shape on ecliptic longitude, latitude, and time. The results of these observations are discussed by Baines et al. (2025). A total of 17 additional background templates were produced from the dedicated SOSS background observations.

For the current analysis an interactive background fitting and subtraction code was used with the 18 available background templates to determine a good background match between each individual observation and the templates. The original templates from Baines et al. (2025) were fit with polynomial functions in the left and right sections to reduce the noise in the templates, as had been previously done for the commissioning template. The code allows the user to examine a rate image and apply different template scaling values. The background-subtracted image rows and an extracted count-rate spectrum can be plotted to aid the user in finding a good match between the different templates and the individual background of the observation under consideration. Although the background subtraction still has some uncertainties because the spectrum of the target takes up a significant fraction of the SUBSTRIP256 subarray, the results are much better than the results from the cycle 1 reductions described in Volk (2024). An automatic background matching and removal algorithm for SOSS mode in the JWST data reduction pipeline is under development, but here the background subtraction was done manually for each observation.

Figure 2 shows an example of the rate image for a particular exposure before and after the background subtraction. The range of values in the display is set to show the region of the maximum of the signal histogram, and so the brighter parts of the object spectra are not displayed in the images.

This background subtraction algorithm is different from an algorithm developed by Tyler Baines which is in the process of being added to the JWST data reduction pipeline at the time this report is being written. It may be necessary to revisit the photometric calibration using the pipeline algorithm once that step is active for SOSS mode in the pipeline. It is hoped that the difference between the current background subtraction algorithm and the pipeline algorithm

will be small.

For some of the cycle 3 photometric observations a dedicated background observation was taken along with the photometric calibration observation. While these observations are shorter than the observations used to make the background templates, they provide a measurement close in time and sky position to the photometric observation. In these cases, the background images were combined into a background template which was used as an alternative to the “standard” templates. The dedicated background seemed to work well for some of the observations, but in other instances the templates produced a better result.

5 Derivation of the Conversion Values

As described previously, the individual spectra were extracted in the JWST pipeline with the `pixel_replacement` step activated, and then a clipped mean spectrum was computed for orders 1 and 2. These spectra are calibrated to units of MJy. For each object the extracted spectra were then compared to the best model spectra available from the STScI CALSPEC page (Bohlin, Gordon, and Trembley, 2014; Bohlin et al. 2022) at <https://www.stsci.edu/hst/instrumentation/reference-data-for-calibration-and-tools/astronomical-catalogs/calspec>. The current “best” spectral models for the five standards were used. The best models have changed since the initial analysis in NIRISS commissioning and the subsequent analysis after the cycle 1 observations were obtained. The names of the models used are given in Table 1 below.

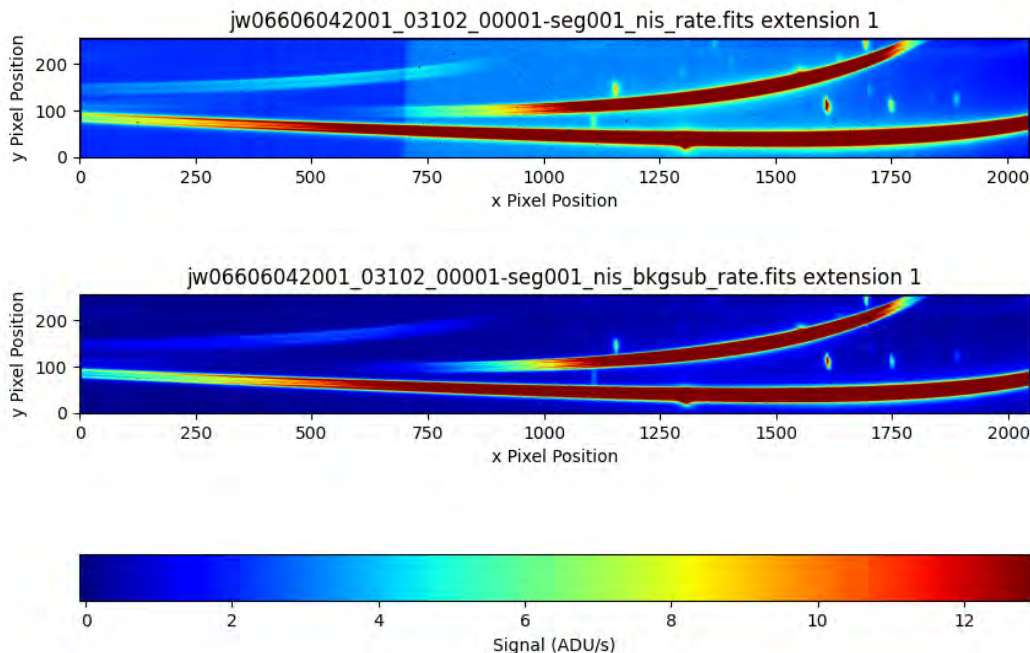


Figure 2: An example of the SOSS background removal. The top image shows the rate image for program 6604 observation 42 of GSPC P330-E. The bottom image shows the background-subtracted rate image on the same display scale, which is linear from 0 to 12.905 ADU/s.

Check with the JWST SOCCER Database at: <https://soccer.stsci.edu>
To verify that this is the current version.

Table 1: A listing of the CALSPEC models used in the determination of the photometric scaling values.

Standard Star	CALSPEC model name
BD+60°1753	bd60d1753_stiswfc_005.fits
2MASS J17430448+6655015	1743045_stisnic_009.fits
G191 B2B	g191b2b_stiswfcnic_004.fits
GSPC P177-D	p177d_stisnic_011.fits
GSPC P330-E	p330e_stiswfcnic_007.fits

The CALSPEC models used combine the Hubble Space Telescope (HST) spectra from observations with the Space Telescope Imaging Spectrometer, Wide Field Camera, and Near-Infrared Camera instruments (as available for the different stars), and these spectra are extrapolated to longer wavelengths using appropriate stellar atmosphere models. The wavelength of the transition from the observed spectra to the stellar models depends on which spectra are available for the star. The values given in the above files were converted from F_λ to F_v and to units of Jansky for comparison with the SOSS spectra.

The SOSS spectra were directly compared to the model spectra, but the main analysis focused on the ratio of the observed spectrum to the model spectrum, with the model interpolated to the wavelengths of the observed spectrum. As the wavelength resolutions of the NIRISS spectra and the HST spectra are similar, an interpolation is sufficient. If the full resolution stellar models from CALSPEC were used instead of the HST-based versions, then one would need to integrate over the model spectrum to match the SOSS wavelength sampling. The hydrogen Balmer, Paschen, and Brackett lines observed in the SOSS spectra have profiles that are different than the profiles in the models and in the HST spectra. When the spectra are divided this produces peaks and troughs in the ratio values around the line positions. Exactly how these appear varies strongly with wavelength depending upon whether the STIS, WFC, NICMOS, or stellar model profile is being divided into the SOSS spectrum. For the Paschen lines between 0.8 and 0.95 μm the STIS profiles are somewhat deeper than the SOSS order 1 profiles, apparently due to the STIS wavelength resolution being better than the SOSS order 1 resolution. This produces roughly 5% peaks at the line positions. At longer wavelengths, the line profile division tends to produce small peaks and larger troughs covering a relative variation of about 10%.

As in the commissioning analysis, the extracted spectrum within the default aperture was compared with the model directly, and no aperture correction was applied. The rationale is that the pipeline uses a fixed aperture for all extractions. If the apertures are correctly positioned on the traces, then the (wavelength-dependent per order) aperture correction will be the same for all these observations and for all the science observations. It is thus assumed that the corrections cancel out and can be ignored. The only concern is that the traces are observed to be rotated slightly within the SUBSTRIP256 subarray for different observations because the NIRISS pupil wheel containing the GR700XD grism can have small variations in the rotation for placing the grism in the light path. This is recorded in the PWCPOS header keyword. The centre of rotation is seen to be different for the different orders, probably because of distortions introduced by the GR700XD grism. Calibration observations to assess the SOSS background

Check with the JWST SOCCER Database at: <https://soccer.stsci.edu>

To verify that this is the current version.

corrections were taken in program 4476. Analysis of this program is ongoing with the photometric analysis presented here and is to be presented in a separate report.

Some of the calibration observations are affected by contamination by spectra from other sources near the photometric standard, due to the slitless nature of the observations. The zero-order spectra are relatively compact and bright compared to the other orders and are more difficult to avoid in general. The presence of contamination was obvious from inspection of the rate images in the background subtraction process.

6 Individual Results

In this section the results for the individual photometric standards are presented. For BD+60°1753 the results from program 1091 are shown but not the many additional measurements from the stability monitoring programs.

6.1 Standard BD+60°1753

The best quality spectrum for this star is from observation 2 of program 1091, which was a test of the time-series observation mode. The signal-to-noise ratio (S/N) of the output spectrum is higher than that for the other standard star observations because a total of 876 integrations were taken. Figure 3 shows the comparison of the output spectra to the stellar model. Figure 4 shows the corresponding ratio plot. The extracted spectra are lower than the model, and the discrepancy becomes larger as the wavelength increases. This is primarily because the previous calibration did not carry out a background subtraction. The effects are larger for order 2 where the signal is generally lower than in order 1, and thus the relative background signal level is higher. In order 2 for wavelengths above 1 μm the spectrum becomes both very noisy and decreases well below the expected values to negative flux densities. This appears to be a result of the ATOCA extraction rather than because of the background subtraction.

Examination of the background-subtracted rate images shows that the signal in the images does not become negative over the order 2 spectrum. Some tests were made offsetting the rate images upwards by small amounts and rerunning the extraction, and this made no difference to the negative values in the extracted order 2 spectra.

At the shortest wavelengths in order 2, shorter than the H α line, the shape of the spectrum is odd, showing a sudden decrease followed by a sharp peak just below 0.6 μm . This general behaviour is observed in all the extracted order 2 spectra, and it does not appear to be directly related to the background subtraction, because these features are too sharp to be the result of the background shape. This is probably due to the ATOCA algorithm having issues where the spectrum is close to the upper edge of the illuminated area of the detector.

The ratio spectra in Figure 4 show that the order 1 ratio values are close to 0.99 at the shortest wavelengths and they are near 0.88 at the long wavelength end. The decline is not uniform. The ratio values are rather flat from the short wavelength end to around 1.24 μm , then the values decrease to 2.0 μm . There is another flat section from 2.0 to 2.35 μm after which the ratio values decline more steeply to the long wavelength limit.

The situation for order 2 is more complex. Aside from the sharp discontinuities in the slope of

Check with the JWST SOCCER Database at: <https://soccer.stsci.edu>

To verify that this is the current version.

the ratio values at wavelengths less than $0.64 \mu\text{m}$, the ratio values dip to 0.975 around $0.7 \mu\text{m}$ and then rise to 1 around $0.8 \mu\text{m}$. After the Paschen series limit the ratio values fall to about 0.875 at $1 \mu\text{m}$. For the longer wavelengths the order 2 spectrum is clearly not reliable and the ratio values fall rapidly to negative values before recovering to positive values that are just below 0.5 at the longest wavelengths. As noted above, much of this is due to the ATOCA extraction. The magnitude of the changes is several times larger than what might be explained by the background signal summed over the extraction aperture.

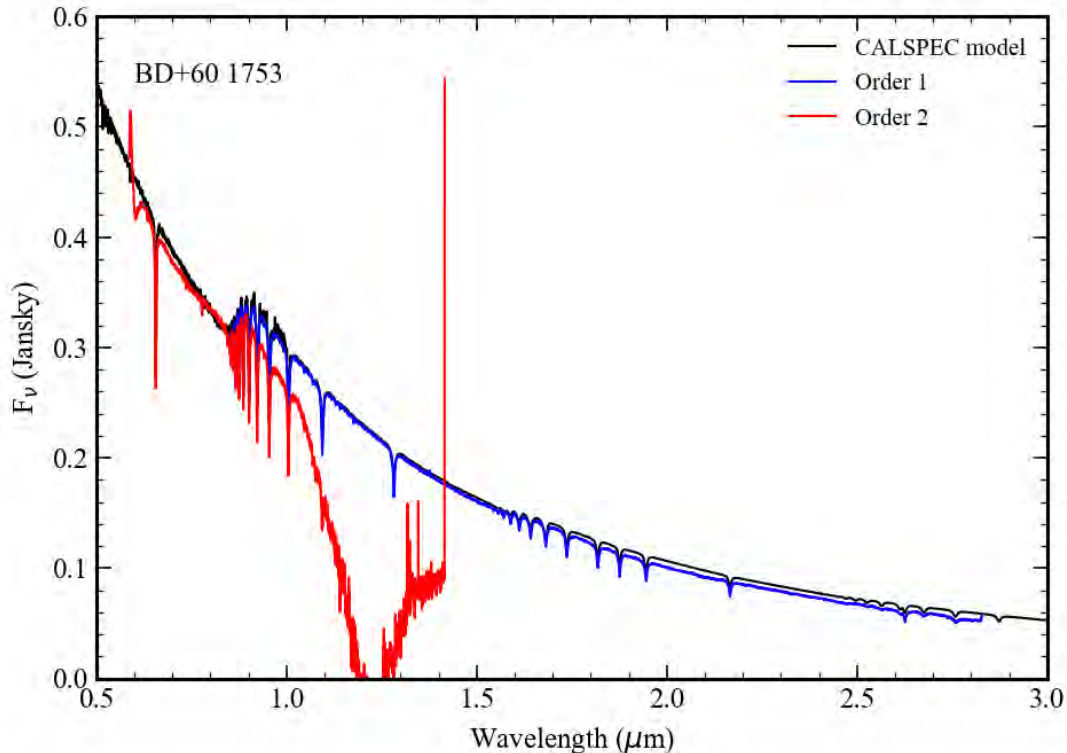


Figure 3: Comparison of the CALSPEC model spectrum of BD+60°1753 to the extracted SOSS order 1 and order 2 spectra.

6.2 Standard 2MASS J17430448+6655015

This star has a spectral type of A8III determined from the STIS spectrum, which is unusual for a photometric standard star. It is close to 4 magnitudes fainter than BD+60°1753. The order 1 spectrum is subject to contamination by a zero-order spectrum that produces a large peak near $1.55 \mu\text{m}$. There is also contamination by a first order spectrum at wavelengths greater than $2.4 \mu\text{m}$. Figure 5 shows the rate image for the observation, and the effects of the contamination.

The source of contamination in the exposure was not identified in the previous analysis of the cycle 1 calibration in Volk (2024). Figure 6 shows the scene image from the Astronomer’s Proposal Tool (APT) for this observation, with the SUBSTRIP256 subarray outlined at the roll angle of the observation. The bright partial spectral orders 1 and 2 in the left part of the rate

image along with the bright zero-order spectrum that is just below the order 1 spectrum of the standard star around pixel 1300 are all due to a single star which is indicated in the ALADIN display.

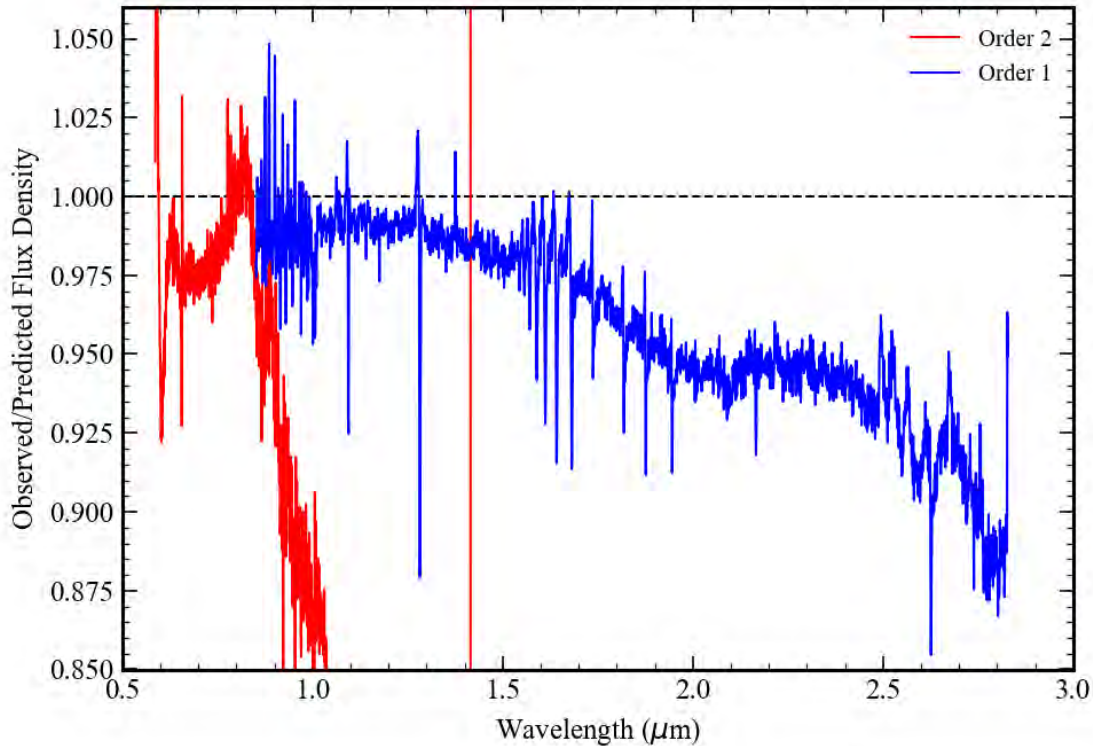


Figure 4: A plot of the ratio of the SOSS order 1 and order 2 spectra to the CALSPEC model values for BD+60°1753. The order 2 spectrum is not reliable for wavelengths greater than 1 μm .

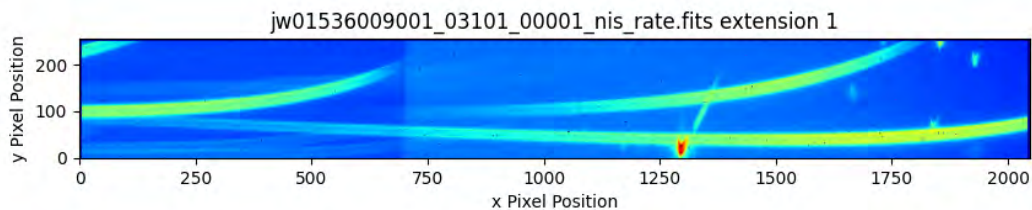


Figure 5: The rate image for the photometric calibration measurement of 2MASS J17430448+6655015. The image is displayed on a logarithmic scale. Comparison with Figure 2 above shows the contamination first order spectrum at left starting at about $y=100$ and the contaminating zero-order spectrum at the lower edge of the subarray near $x=1300$. The zero-order contamination also crosses order 2.

Check with the JWST SOCCER Database at: <https://soccer.stsci.edu>
To verify that this is the current version.

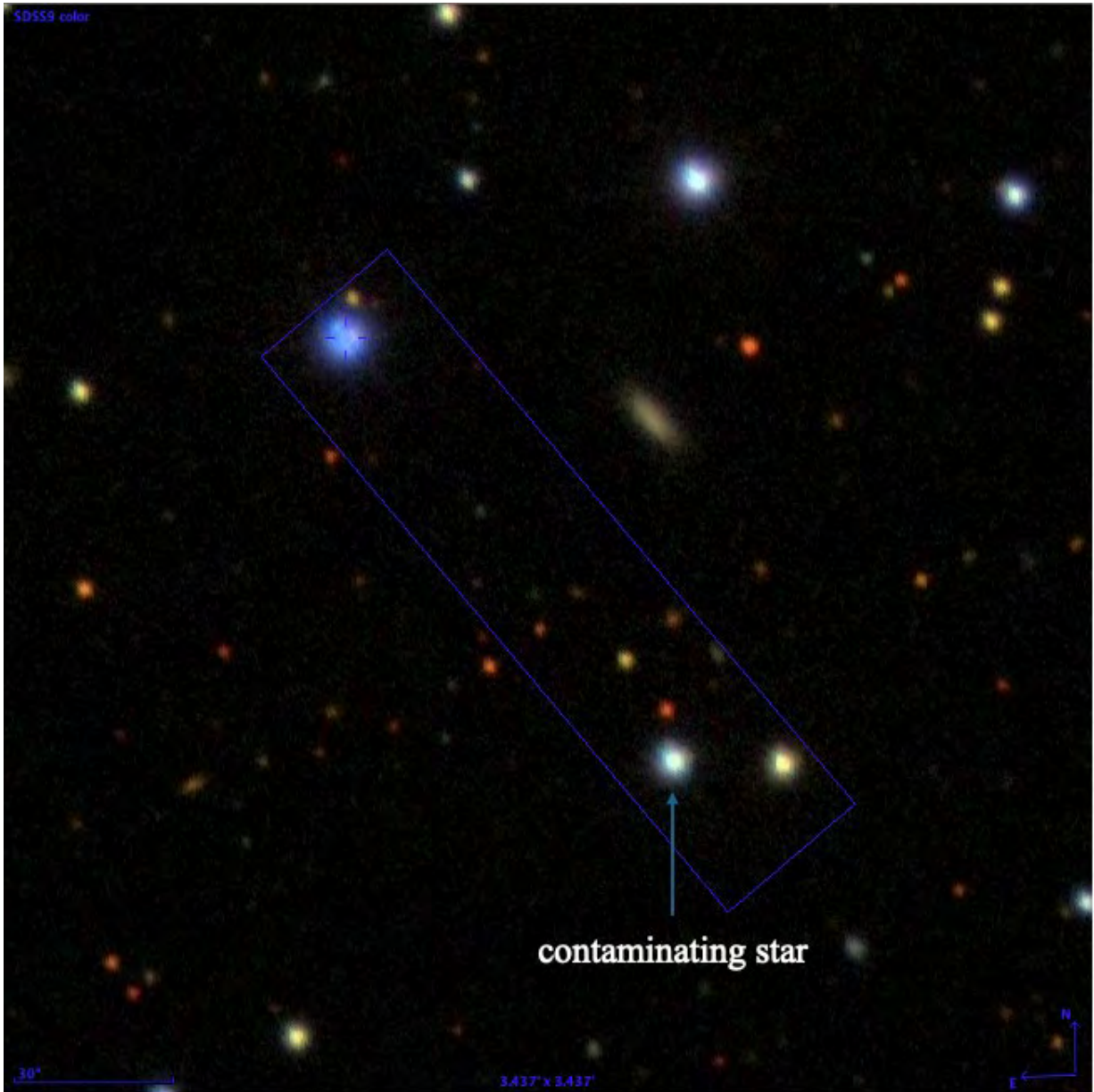


Figure 6: Illustration of the field around 2MASS J17430448+6655015 showing the orientation of the SUBSTRIP256 subarray for the photometric observation (blue rectangle). The blue arrow points to the star that is producing the brightest zero-order and first order spectral contaminations in the exposure.

The contaminating spectra are from star Gaia DR3 1634280277840964864, which has no SIMBAD association. The observation roll angle happened to be unfavourable by chance. For most roll angles the contamination would have been much less than what is seen in the observation. Photometry values for the contaminating star in comparison with 2MASS J17430448+6655015 are given in Table 2. The Gaia DR3 astrophysical parameters for this star are $T_{\text{eff}}=5415$ K, $\log_{10}(g)=4.173$, and $[M/H]=+0.122$, which suggests a spectral type of about G3 IV.

Table 2: Magnitudes for 2MASS J17430448+6655015 compared to those for the two main contaminating stars in the photometric observation.

Filter	2MASS J17430448+6655015	Gaia DR3 1634280277840964864
SDSS u	14.7614±0.0036	16.8046±0.0073
SDSS g	13.5448±0.0024	15.1682±0.0026
SDSS r	13.4943±0.0027	14.6268±0.0028
SDSS i	14.0835±0.0064	14.4753±0.0030
SDSS z	13.6327±0.0033	14.4203±0.0038
Gaia DR3 G	13.4711±0.0002	14.6828±0.0002
Gaia DR3 G _{rp}	13.6078±0.0006	15.0591±0.0008
Gaia DR3 G _{rp}	13.2368±0.0004	14.1488±0.0007
2MASS J	12.979±0.018	13.527±0.0026
2MASS H	12.880±0.023	13.248±0.0027
2MASS K _s	12.772±0.026	13.092±0.0034
WISE W1	12.822±0.022	13.128±0.023
WISE W2	12.856±0.022	13.171±0.023
WISE W3	12.663±0.027	13.048±0.312
WISE W4	> 9.692	> 9.791

The comparison of the SOSS spectra to the CALSPEC model spectrum and the resulting ratio values are plotted in Figure 7 and Figure 8. The order 1 spectrum agrees with the CALSPEC spectrum out to a wavelength of about 1.9 μm . It appears that the CALSPEC spectrum is of lower S/N in the wavelength range of the NIRC MOS spectrum, from 1.01 to 2.38 μm . The zero-order contamination produces the peaks at 0.77 μm in order 2 and 1.55 μm in order 1. The order 2 spectrum appears to be of good quality out to about 1.1 μm , beyond which the spectral values become much larger than the model prediction. For the order 1 spectrum there may be issues starting at 1.9 μm . It is possible that the background subtraction is not quite correct, and this may cause the small dip at 2.15 μm and the small excess from there to 2.4 μm . At the longer wavelengths the spectral shape is peculiar because of the contamination with the second order 1 spectrum seen in Figure 5. There are also the two faint contaminating traces near the bottom of the subarray out to column 750, but these appear to be too faint to cause the variations that are seen out to 2.4 μm .

The ratio values in Figure 8 are close to 1.0 for order 2 out to the Paschen series limit, at which point they decrease to about 0.96 by wavelength 0.91 μm . After that the values decrease by a few more percent to wavelength 1 μm but then rise so that at wavelengths greater than 1.05 μm the extracted spectrum is well above the model. The shape of the ratio values at longer wavelengths (out of the plot range in Figure 8) is the same as the shape of the dip to negative values seen for the order 2 spectrum of BD+60°1753 but has the opposite sign. This is probably primarily due to the ATOCA extraction in the wavelength range where the order 2 signal is very low.

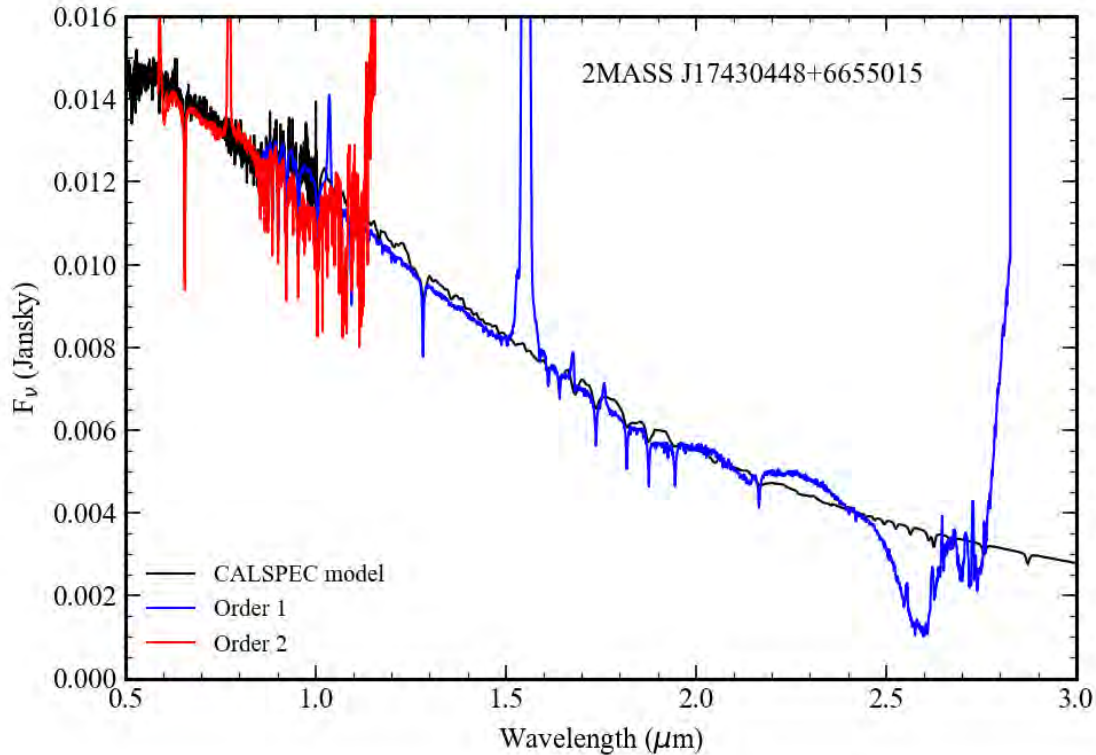


Figure 7: Comparison of the extracted SOSS order 1 and order 2 spectra to the CALSPEC model spectrum of 2MASS J17430448+6655015. The zero-order contamination produces the feature at about 1.55 μm in the order 1 spectrum. There may be issues with the background subtraction that are affecting the order 1 spectrum from 2.15 to 2.4 μm , but there is also overlap with the contaminating order 1 spectrum that produces the unusual shape for wavelengths greater than 2.4 μm . The order 2 spectrum is unreliable at $>1.1 \mu\text{m}$. The peak at about 0.77 μm is due to the same zero-order contamination as in order 1.

For order 1 the ratio values outside the line cores are between 0.97 and 1 for wavelengths out to 1.65 μm except where there is contamination. At longer wavelengths the ratio values are in the range from 0.96 to 1.0 out to 1.97 μm , after which the values rise to 1.1 at about 2.28 μm and then start to decline. The structure on order 1 from 2.15 to 2.4 μm may be due to limitations in the zodiacal background subtraction, since there is a narrow dip in the spectrum at the position of the background discontinuity and then a broad low amplitude excess to longer wavelengths. The structure of the spectrum beyond 2.4 μm is clearly untrustworthy due to the contamination from the additional first order spectrum. These long wavelength features were also seen in the extractions from the previous analysis reported in Volk (2024) but the results here have much better S/N and much less background-related structure at the short wavelengths.

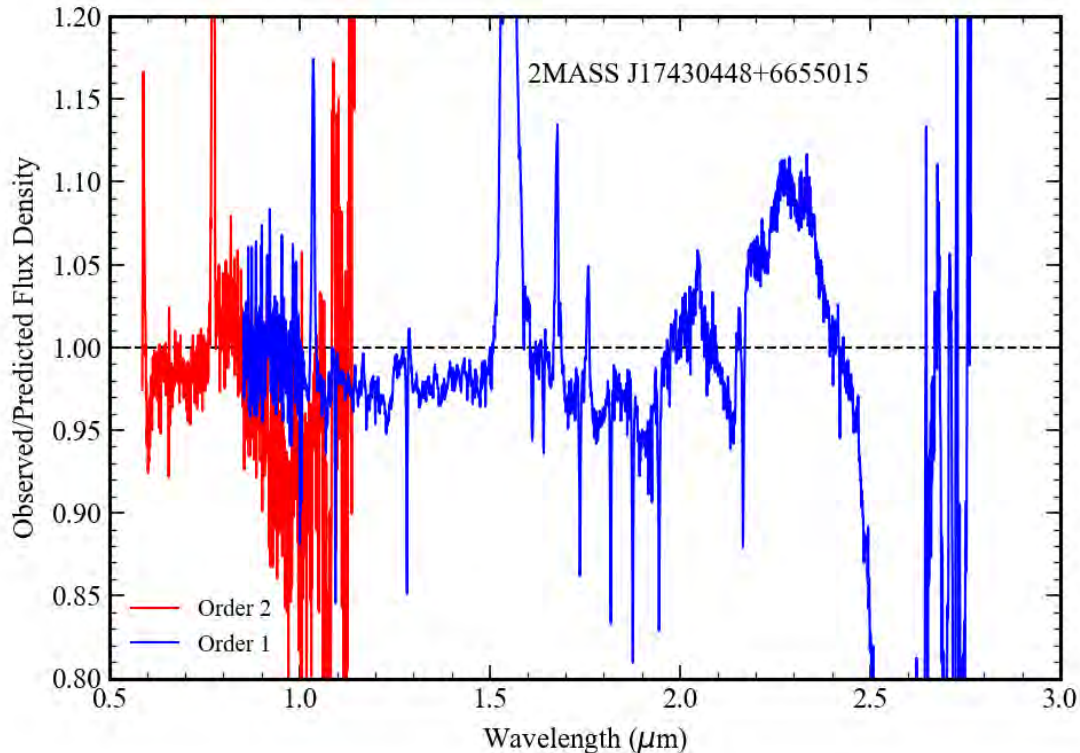


Figure 8: The ratio of the observed spectra to the CALSPEC model spectrum for 2MASS J17430448+6655015. It appears that the order 1 ratio values are not useful above 1.9 μm , and it is not clear how much of the ratio information from 1.5 to 1.9 μm is of good quality. For order 2 the ratio values become unreliable at wavelengths above about 0.9 μm .

6.3 Standard G191 B2B

The SOSS observation of this star is subject to some contamination as is discussed by Volk (2024). There are some relatively faint zero-order spectra that affect the order 1 spectrum, and there is a contaminating spectrum at the longer wavelengths. For this target the field is sufficiently crowded that contamination is unavoidable, but it was important to observe it as it is one of the primary HST calibration standards. The SOSS spectra are compared with the CALSPEC mode in Figure 9, and the ratio values are presented in Figure 10.

The order 1 spectrum shows the Pa α and Pa β lines. The line shapes resemble those in the HST STIS/WFC spectra. There are seven peaks from contamination at wavelengths 0.8536, 1.116, 1.248, 1.337, 1.350, 1.708, and 2.004 μm . For wavelengths larger than 2.4 μm the contamination affects the extracted spectrum. In order 2 the H α line is present, again matching well to the HST STIS profile, and there are small contamination features at 0.6584 and 0.7494 μm . At wavelengths larger than 1.01 μm the order 2 spectrum shows a large excess signal, similar to what was seen for 2MASS J170430448+6655015, which presumably is caused by the contaminating spectrum that also affects order 1.

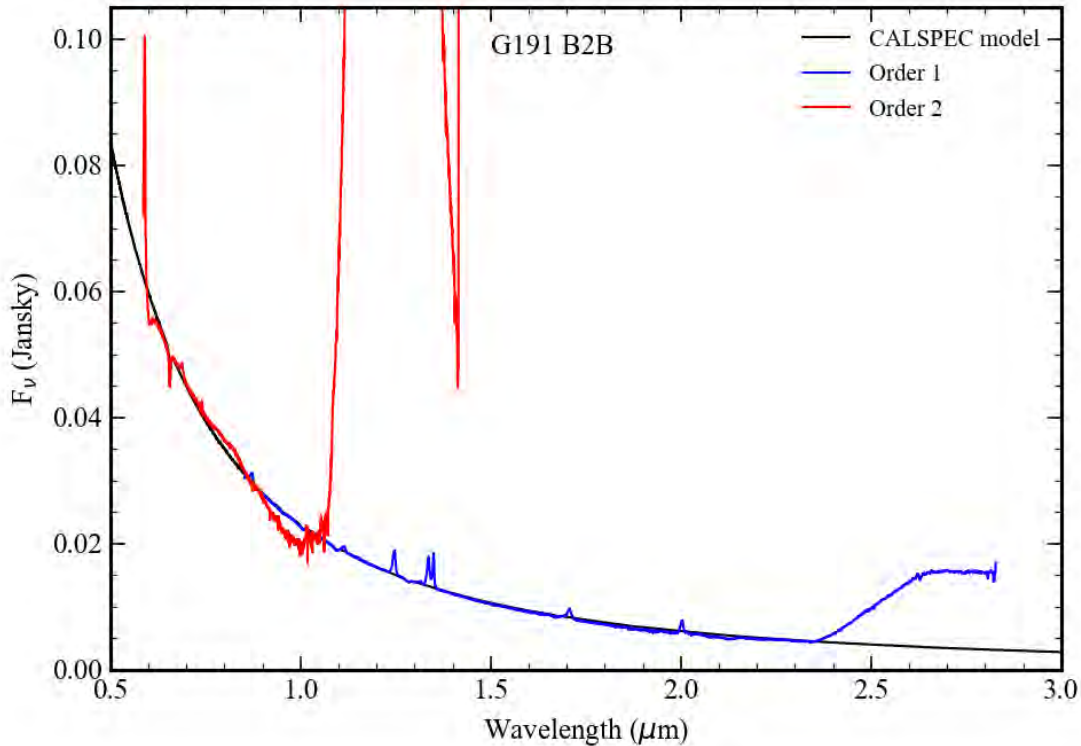


Figure 9: Comparison of the extracted SOSS spectra with the CALSPEC model for G191 B2B. Both SOSS orders are affected by contamination at the longer wavelengths. In addition, the small bumps on the spectrum such as at 1.337 and 1.350 μm are due to contamination.

The short wavelength part of the order 2 spectrum shows some interesting properties. The ratio is around 0.99 for wavelengths from 0.861 to 0.893 μm , but then the ratio values rise to a peak of 1.05 at about 0.821 μm and then decline to a value of 1 just before the $\text{H}\alpha$ line. It appears that there is some type of small mismatch in the $\text{H}\alpha$ line position in the SOSS spectrum because the ratio values go up to 1.02 and then rapidly down to 0.97 over central part of the $\text{H}\alpha$ line profile. On the short wavelength side of the $\text{H}\alpha$ line the ratio is at about 0.98 until 0.6184 μm , then the ratio declines to a minimum of 0.92 at 0.6025 μm before the ratio rises to a peak of 1.63 at 0.5905 μm and declines again towards the short wavelength limit. This peak at ≈ 0.59 μm is both significantly higher than and somewhat wider than the short wavelength peaks seen in the other standard ratio spectra.

6.4 Standard GSPC P177-D

In this case a clean spectrum was obtained with little in the way of contamination issues. There are some zero-order spectra in the rate image. One of these is located at $x=729$, $y=77$ with a peak count rate of about 5 ADU/s. This is in between order 1 and order 2 at that position along the traces and seems to be of most concern for the extracted spectra. Two other zero-order spectra are brighter but are also further away from the traces.

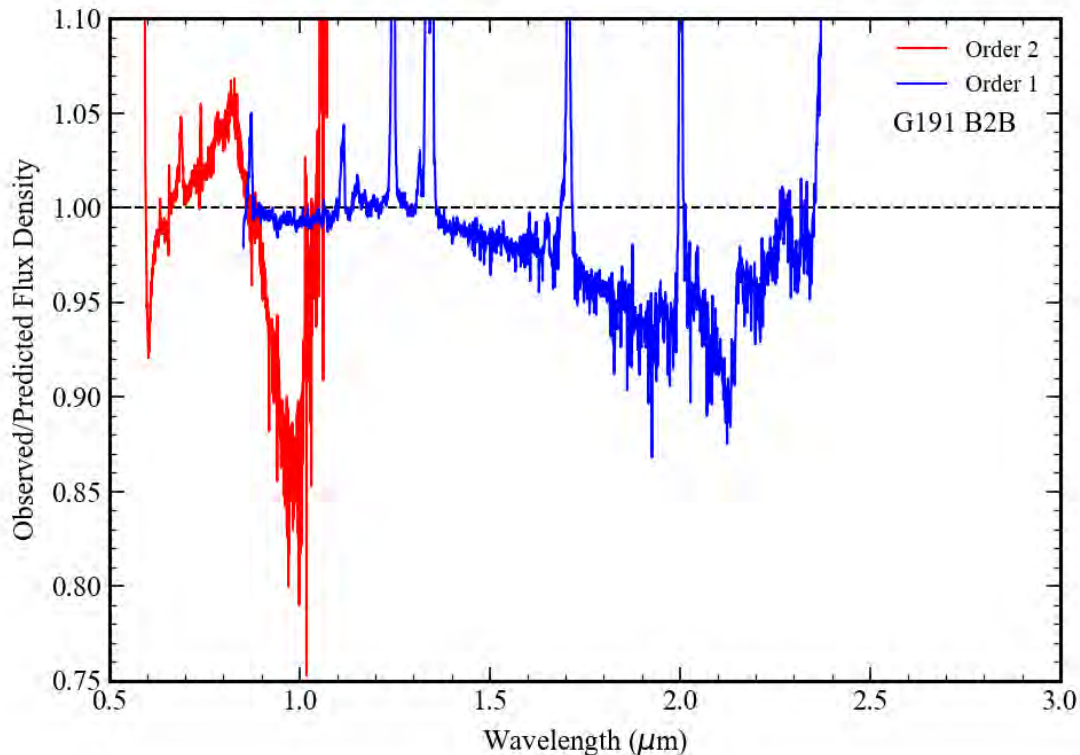


Figure 10: The ratio of the observed spectra to the CALSPEC model for G191 B2B. The order 2 spectrum shows a narrow peak up to a ratio value of 1.63 which is not shown in this plot. Both SOSS orders have contamination at the longer wavelengths from a contaminating spectrum, which are also not shown here. The various narrow peaks such as at 1.337/1.350 μm are due to contamination from zero-order spectra.

The comparison of the extracted SOSS spectra to the CALSPEC model spectrum is shown in Figure 11, and the ratio plot is shown in Figure 12. This star is solar-like with spectral type G0V. A few absorption lines are seen in the SOSS spectra including H α , Pa α , and Pa β . For the wavelength range where the CALSPEC model is based on NICMOS data these lines are generally not obvious in the model spectrum. The contamination from the zero-order spectrum mentioned previously can be seen in order 1 at 2.115 μm and in order 2 at 1.068 μm . There are other peaks in the ratio spectra that appear to be due to order zero contamination although the causes are not immediately obvious from examining the rate image.

The order 1 ratio values are close to 1 at the shortest wavelengths and decline to a value of about 0.85 at the long wavelength end. The relative shape resembles what is seen for BD+60°1753 in Figure 4, although the overall amplitude is a little larger here. The order 2 ratio values in the plot are also similar to the values in Figure 4 out to about 0.9 μm , but the curves are different for wavelengths greater than 1 μm .

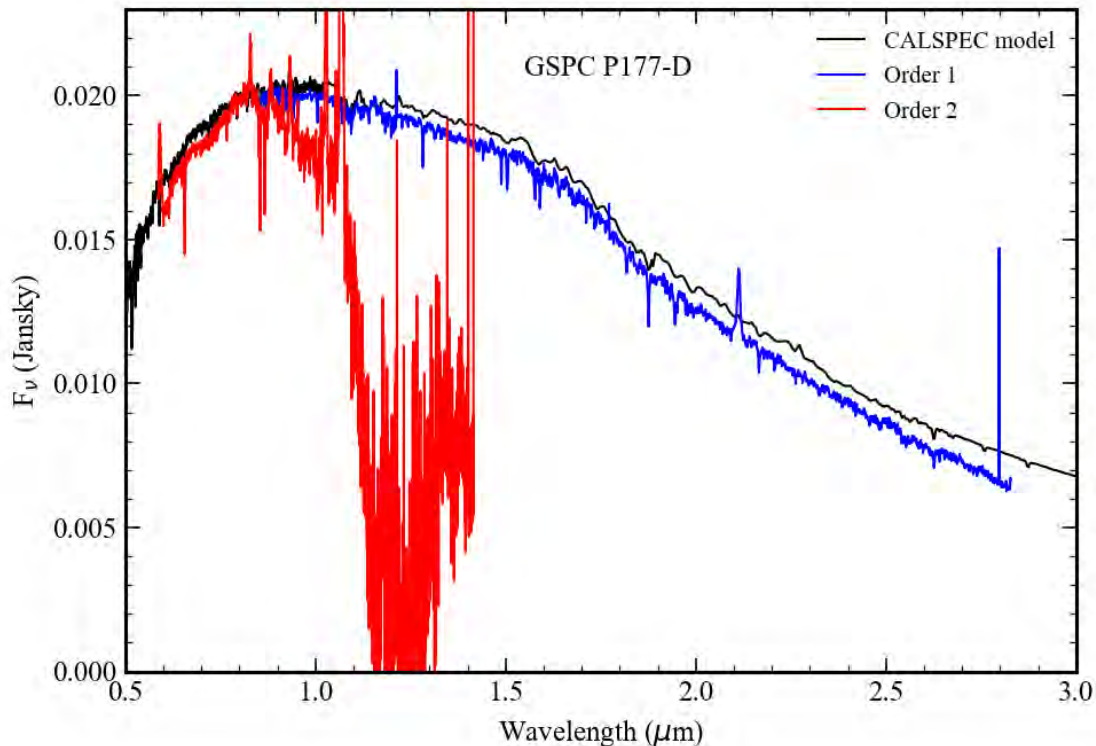


Figure 11: Comparison of the extracted SOSS spectra with the CALSPEC model for GSPC P177-D.

6.5 Standard GSPC P330-E

There are three SOSS observations of GSPC P330-E available, a single observation in cycle 2 and two observations in cycle 3. In the last of these observations a dedicated SOSS background observation was added to the program to improve the calibration results. Examination of the rate images shows that there are some faint zero-order spectra near or on the traces in all three observations, but that the situation is better for the cycle 2 observation. Program 6606 observation 42 shows an order zero spectrum on the order 1 trace at $x=1303$, $y=34$. For observation 24 there is a zero-order spectrum just above the order 1 trace at $x=700$, $y=71$, and another on the order 2 trace at $x=1019$, $y=115$. For the observation in program 4498 there are only very faint order zero spectra visible at 1 to 3 ADU/s above the background, and there is a faint order 1 spectrum seen on the left part of the subarray that crosses the standard star order 1 trace at about $x=420$, which is roughly 20 times fainter than the GSPC P330-E spectrum at that point.

Figure 13 shows the comparison of the output SOSS spectra from the three observations with the CALSPEC model. All three sets of SOSS spectra are generally below the CALSPEC model over most of the wavelength range. It is also seen that the general shapes of the three independent observations are very similar in orders 1 and 2, although with some variation seen at the longer wavelengths in both cases. In both the program 6606 order 1 spectra there is some contamination by a zero-order spectrum at a wavelength around $2.05 \mu\text{m}$. The extracted spectrum from program 4498 has a broad hump between about 2.1 and $2.6 \mu\text{m}$ that is not

observed in the other spectra. Although it might be thought that this is due to the relatively faint contaminating order 1 spectrum seen in the rate image, that spectrum is present at $x < 420$, which is at longer wavelengths than those where the feature is seen in the extracted spectrum. Going back to examine the rate image did not show any source of contamination that would explain an excess out to $x=700$ as is observed in the order 1 spectrum.

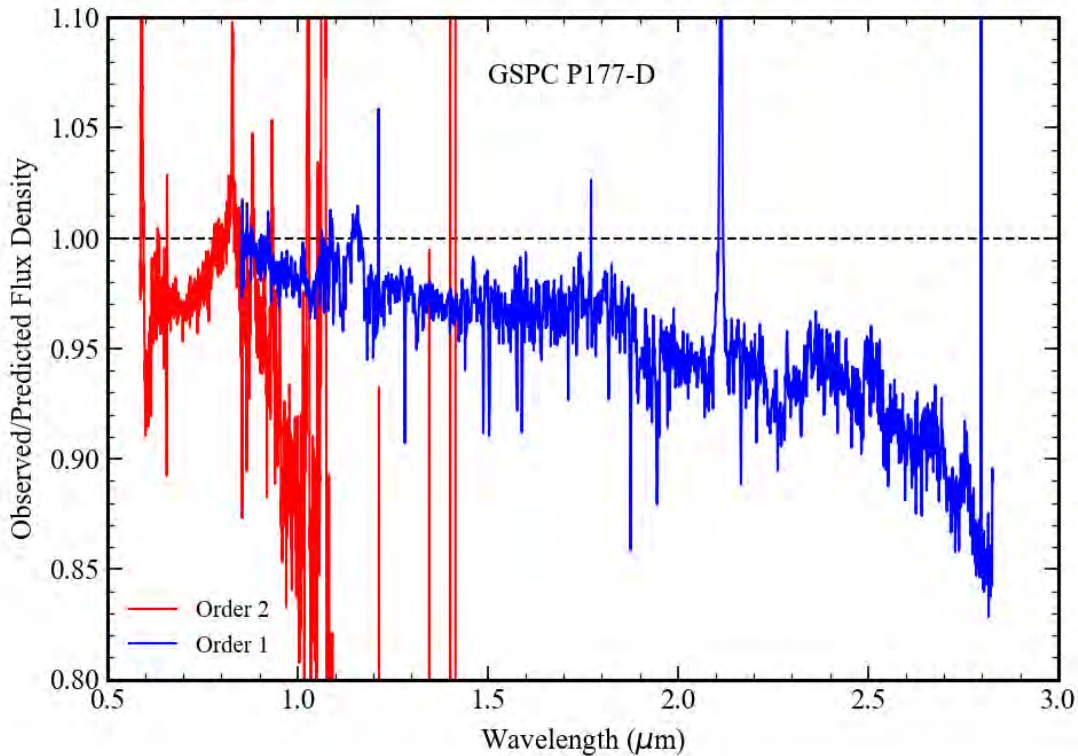


Figure 12: The ratio of the observed spectra to the CALSPEC model for GSPC P177-D.

The ratio values for the three observations are presented in Figure 14. They have similar shapes in the three cases, modified somewhat by the broad peak in the 4498 order 1 spectrum at the longer wavelengths of order 1, but the level at the longest wavelengths varies somewhat between the three observations. There are also variations in detail for the order 2 ratio spectra, especially some changes in the amplitude of the narrow peak at the shortest wavelengths between the three observations. The plot range in Figure 14 does not show the peak value at short wavelengths for the 4498 observation.

The order 2 ratio values for the three observations differ at wavelengths greater than 1.1 μm . All three show a similar shaped large bump but the amplitude varies significantly between the observations, with the bump being only modest for the 4498 observation.

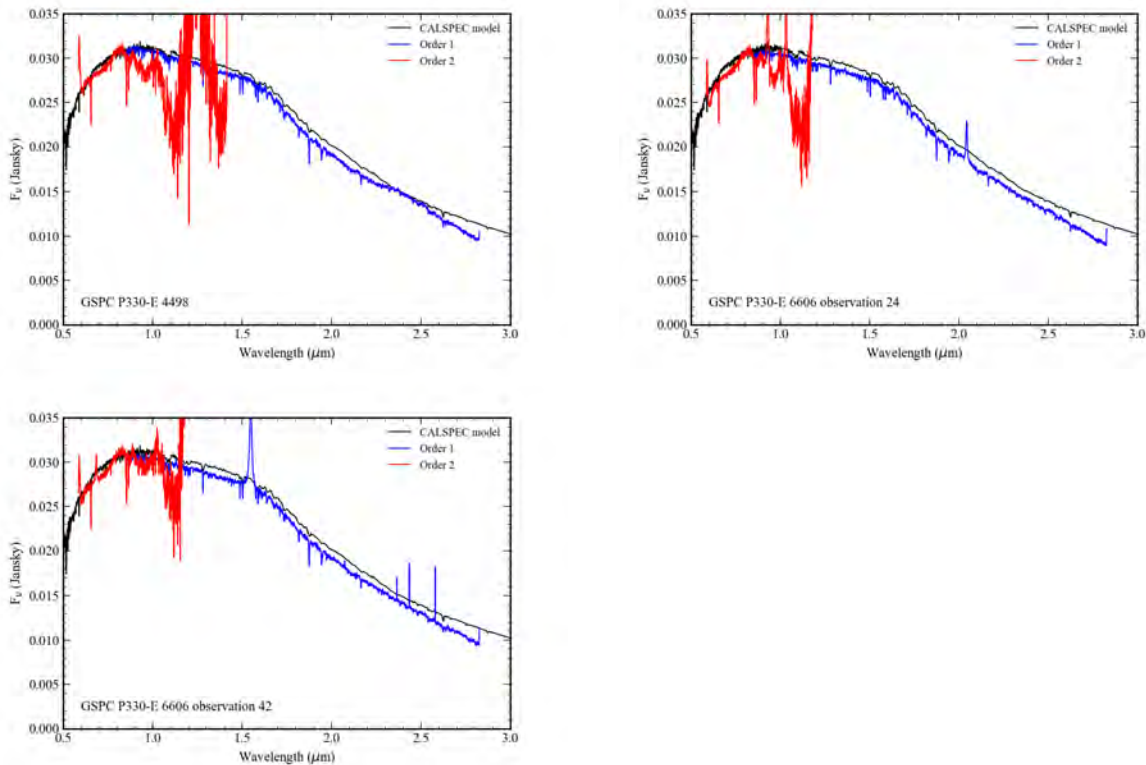


Figure 13: Comparison of the extracted SOSS spectra for GSPC P330-E with the CALSPEC model spectrum. The three extracted spectra are from cycle 2 program 4498 and cycle 3 program 6606 observations 24 and 42.

7 Combining the Conversion Values

Having obtained the ratio spectra for the different observations the next task is combining these to produce the correction values that need to be applied to the current SOSS photometric calibration values. The question of how to combine the different ratio spectra depends upon what assumption is made about the nature of the variations seen from one object to another. One possibility is that the variations are purely statistical in nature, in which case a weighted mean based on the exposure times would be a suitable method of averaging. Another possibility is that the variations are systematic, primarily being caused by the limitations of the background subtraction or in the CALSPEC models, in which case a simple unweighted mean would be the best choice. It is obviously possible that both statistical and systematic errors are present in the ratio spectra, in which case there is no simple algorithm for producing the correct mean values.

There is clearly some statistical uncertainty component in the ratio values as is seen in the pixel-to-pixel variations in the ratio spectra. For order 1 this component is roughly constant across the wavelength range, while for order 2 it clearly gets larger at the longer wavelengths. To remove this variation, low-order Legendre polynomial or cubic spline fits were carried out to approximate the order 1 and order 2 ratio spectra in a smooth manner, over the regions that are judged to be uncontaminated. Legendre polynomial fits were attempted first and if those did not produce a good result the cubic spline fits were carried out. For G191 B2B and 2MASS J17430448+6655015 the order 1 spectra were truncated to exclude the long wavelength part that is

Check with the JWST SOCCER Database at: <https://soccer.stsci.edu>
To verify that this is the current version.

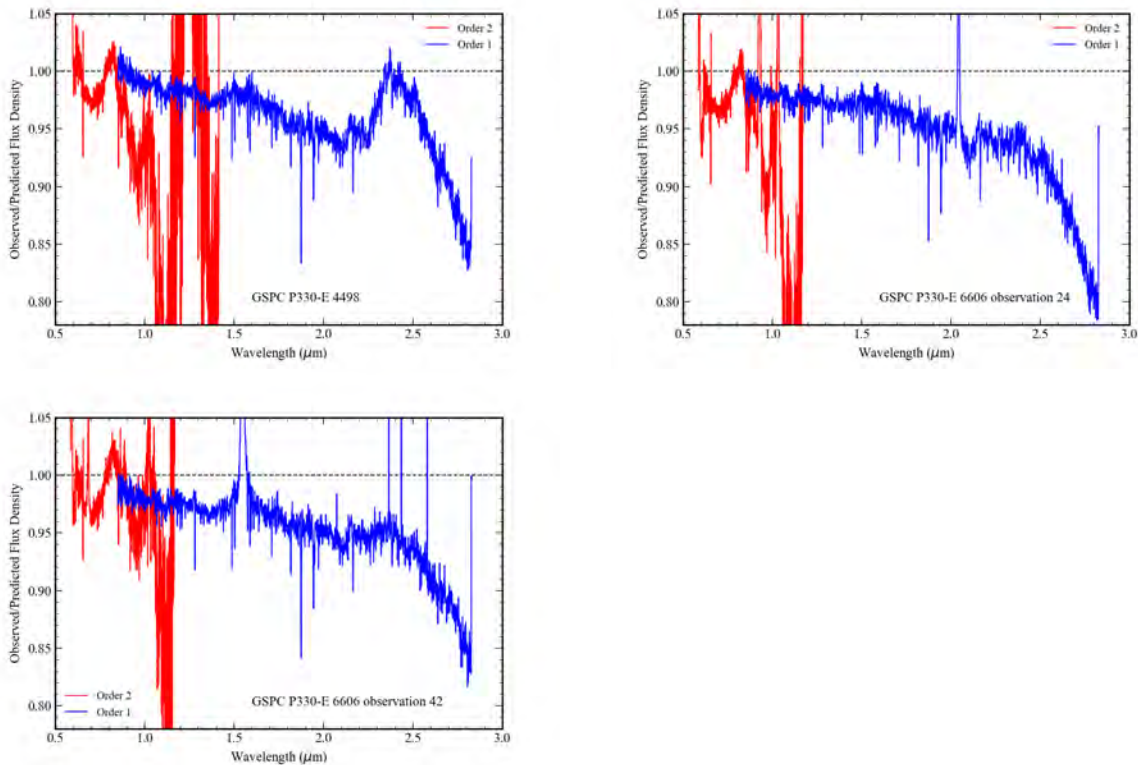


Figure 14: The ratio of the observed spectra to the CALSPEC model for the three observations of GSPC P330-E.

contaminated before doing the fitting. In the case of order 2 the fitting needed to be done in several sections because of the breaks in the values caused by the sharp peak seen at the short wavelengths in all the spectra. This sharp peak was fit using linear or quadratic fits over the range from the short wavelength end to the peak and from the peak to the minimum around $0.60 \mu\text{m}$. A normal fit was made to the longer wavelength order 2 ratio values, and then some manual adjustment was made to allow the curves to join up properly. For BD+60°1753 the ratio spectra for the photometric stability observations were combined pixel-by-pixel using the `astropy sigma_clipped_stats` routine with a 3σ rejection threshold and up to 5 iterations, which gave a good result since most of the order 1 observations were not subject to much contamination. The mean ratio spectra were compared to the 1091 ratio spectra and they agreed well. Then a fit was made to the mean values in the same way as for the other observations. This produced a total of eight fitted functions in order 1, the two for BD+60°1753 plus three for GSPC P330-E, and one each for the other standards. Plots of the fits for orders 1 and 2 are shown in Figure 15.

Considering order 1 first, it appears that the results for G191 B2B and 2MASS J17430448+6655015 are anomalous, especially for the latter star. At wavelengths less than $2.1 \mu\text{m}$ the spread between the different fit curves is generally at the 2% to 2.5% level, although the agreement is at the 1% level around $2 \mu\text{m}$ except for the values for G191 B2B. There is more variation at the longer wavelengths, and the spread is about 11% at the longest wavelengths.

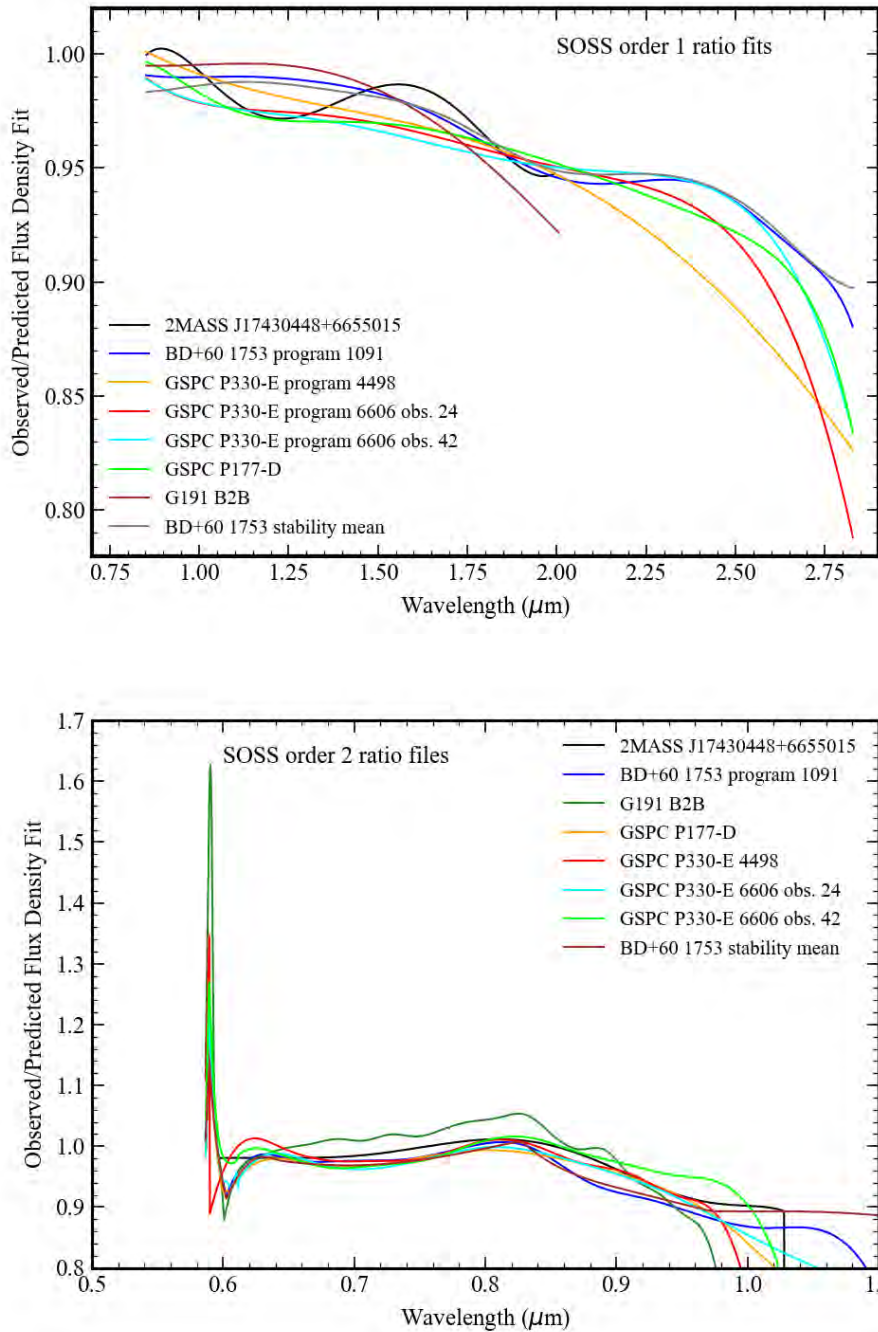


Figure 15: The fit functions for the first and second order spectra from different standard star observations. For 2MASS J17430448+6655015 and G191 B2B the first order spectra were limited to the range up to 2.0 μm. For the cycle 2 first order observation of GSPC P330-E the wavelength range between 2.1 and 2.6 μm was excluded because the bump observed at these wavelengths was not present in the cycle 3 observations.

There is more variation between the different fits for order 2 than for order 1. The results for G191 B2B are again different than what is obtained from the other standards. The fit for

Check with the JWST SOCCER Database at: <https://soccer.stsci.edu>
To verify that this is the current version.

2MASS J17430448+6655015 is cut off at 1.023 μm because of contamination. For the central wavelengths of order 2 between 0.61 and 0.84 μm the different curves show roughly 2% variation excluding G191 B2B or about 4% including all the stars. There is much more dispersion in the values below 0.61 μm and the position of the break where the short wavelength peak starts varies over about 0.07 μm . The peak value has a large range from 1.14 to 1.35 for the stars other than G191 B2B. For the latter star the peak is at 1.63 and the peak is wider than in the other cases. There is also a fairly large range in the wavelengths where the ratio values turn sharply downwards in the individual spectra, from 0.975 to 1.105 μm .

The individual ratio values were averaged in two ways to produce mean ratio values for orders 1 and 2. In the first method the ratio functions were averaged using the `astropy sigma_clipped_stats` routine with a threshold of 3σ and a maximum of 5 iterations. This would be the best method if the variations are systematic, either from limitations to the standard star models or because of the background subtraction. The second method used a weighted mean of the values, with the weight being the square-root of number of frames contributing to the mean extracted spectrum. If the different observations reached the same maximum total counts at each wavelength, then this provides an approximation to Poisson uncertainties. It would be difficult to estimate the Poisson noise in the individual spectra because of the complications of the ATOCA extraction.

The clipped mean calculation was done both on the raw values and on the fit curves. It was found that there are small discontinuities in the mean of the fit values in order 1 at a few discrete wavelengths, presumably because of changes in the number of sources included after the sigma clipping. There was an offset of about -0.03% around 1.995 μm and a larger offset of $+0.29\%$ around 2.005 μm . As there was no sharp change in shape just the small offset these were removed by scaling to the shorter wavelength section in each case. The weighted mean values did not show such offsets.

For order 1 the difference between the clipped mean function and the weighted mean function is less than 0.1% for wavelengths between 0.85 μm and 0.957 μm as well as for wavelengths between 1.75 μm and 2.2 μm . In between the difference is about 0.3%. The difference rises to $+2\%$ at wavelengths greater than 2.3 μm .

The situation for order 2 was much more complicated. There were many offsets in the mean values as a function of wavelength, again apparently because of variations in which stars were contributing to the mean values. The values were clearly untrustworthy for wavelengths greater than 1.1 μm . The offsets were reduced when the sigma clipping threshold was set to $+2\sigma$ on the high side, but they were not entirely removed. For order 2 the offsets at longer and shorter wavelengths were removed by matching to the values between 0.74 and 1.0 μm where the S/N is the highest; there was only one small offset section close to 0.85 μm within that wavelength range. For wavelengths beyond 0.95 μm the mean values become relatively inaccurate, and beyond about 1.1 μm they are not reliable. The ratio values for the commissioning observation of BD+60°1753 were used at wavelengths beyond 0.9525 μm where the mean values turn sharply downwards. Once the shifting was done, the weighted mean and clipped mean values agreed within 1% over the order 2 wavelength range. The final

ratio values for the two orders and the two types of averaging are shown in Figure 16.

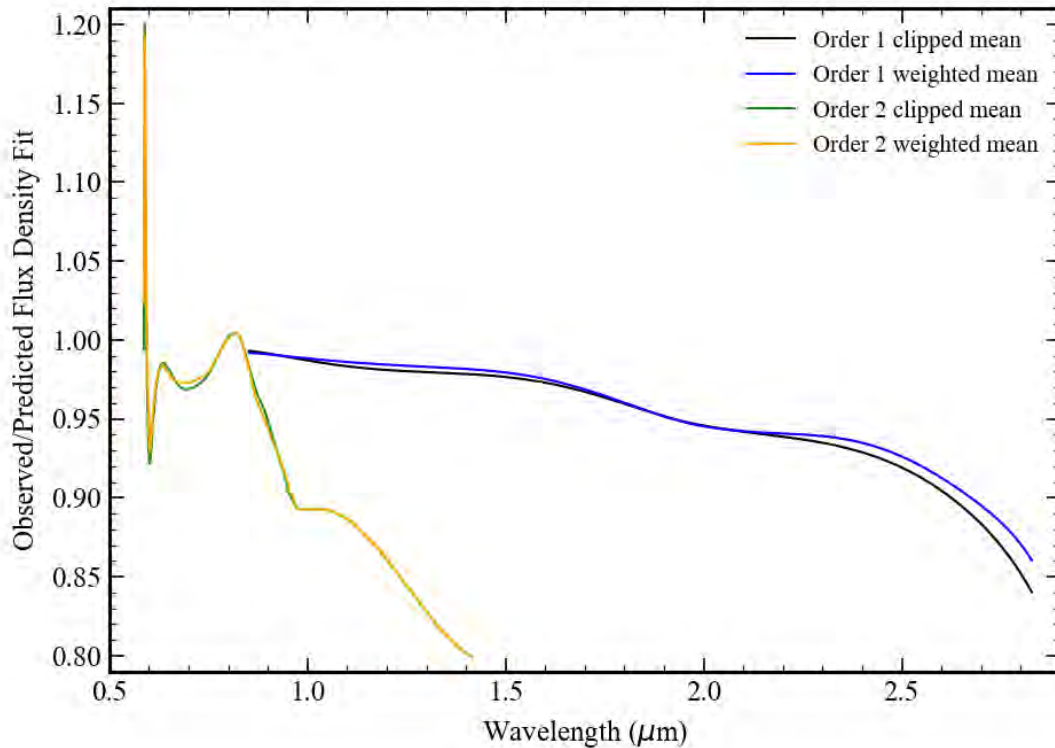


Figure 16: The final mean ratios of the observed to predicted flux density values for the SOSS order 1 and order 2 spectra using either the clipped mean or the weighted mean to generate the values.

8 A Test of the New Conversion Values

Having obtained the ratio values from the analysis of the standard star observations, a test was made on an independent data set. The cycle 1 calibration program 1516 observed star HD 59533 in SOSS mode to evaluate the effects of charge migration on the SOSS extracted spectra (see Goudfrooij et al. 2024 for a description of charge migration in the imaging case). This provides a good S/N spectrum of a single star which can be used as a test of the calibration.

Observation 6 of program 1516 was reduced in the same way as was done for the photometric standards, with background subtraction using the available templates. The extracted order 1 and order 2 spectra were then scaled by the weighted mean ratio values shown in Figure 16 above.

The photometry for this star was obtained from the Vizier photometry page (<http://vizier.cds.unistra.fr/vizier/sed/>; Ochsenbier, Bauer, and Marcout, (2000)) with a search radius of 1.0". In addition, there is a Gaia prism spectrum for this star in Gaia Data Release 3 (Gaia Collaboration et al. 2013, Gaia Collaboration et al. 2023) that was obtained from the

Gaia archive. The Gaia stellar parameters listed for this star are $T=8052$ K, $\log_{10}(g)=3.897$, $[M/H] = -0.897$, and $A_G=0.12$. Taking these values as a guide, a Phoenix grid model from Husser et al. (2013) with parameters $T=8000$ K, $\log_{10}(g)=4.0$, $Z=-1.0$, and $\alpha=0.0$ was used as a base model. The Phoenix model was smoothed to a resolution of 1000, scaled to the 2MASS K_s magnitude of the star, and then compared with the available photometry and the Gaia prism spectrum to determine the reddening. A revised version of the extinction curve from Rieke and Lebofsky (1985) was used for the reddening function. The best match was found with $A_V=0.09$, which is reasonably consistent with the Gaia A_G value. The reddened model was then used to make SOSS ratio spectra in the same way as what was done with the CALSPEC models and the photometric standard observations. Figure 17 shows the direct comparison of the Phoenix model spectrum to the Gaia prism spectrum and the SOSS spectra. Figure 18 shows the corresponding ratio plot.

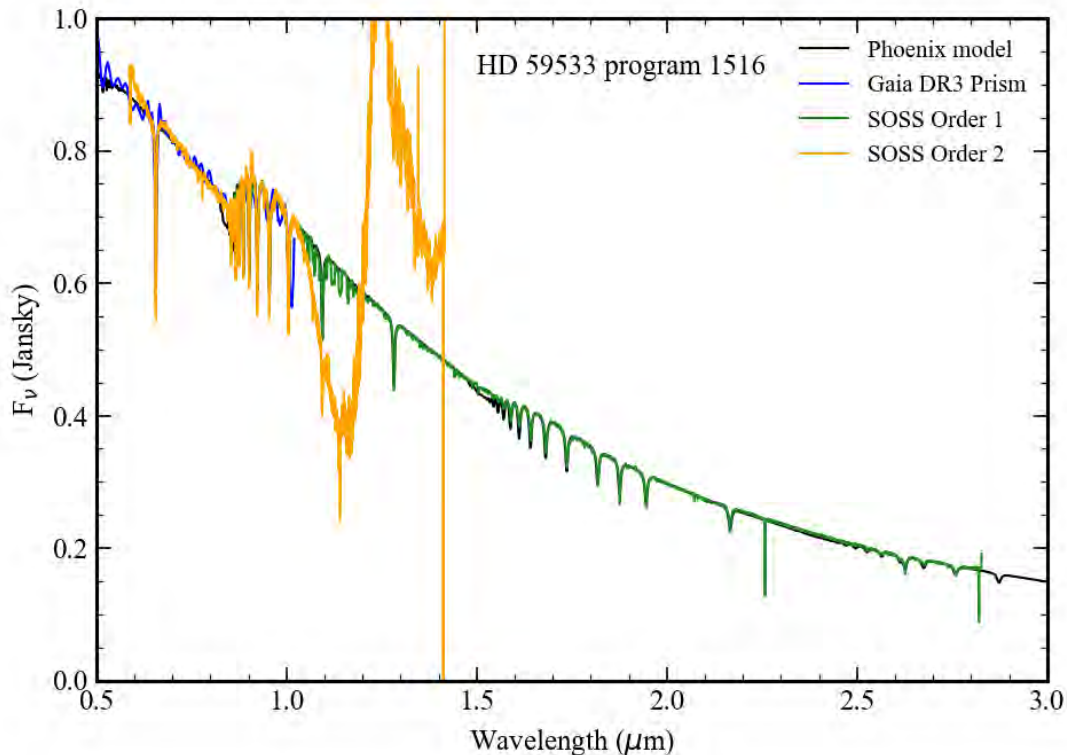


Figure 17: Comparison of the Phoenix grid model from Husser et al. (2013) for $T=8000$ K, $\log_{10}(g)=4.0$, $Z= \times 1$, and $\alpha=0.0$ with the SOSS spectra and Gaia prism spectrum of HD 59533. The stellar model has been reddened with $A_V=0.09$ magnitudes and scaled to the 2MASS K_s brightness.

As was seen for the CALSPEC models, the Hydrogen line profiles in the model spectrum do not exactly match the profiles in the SOSS spectra, so the ratio values decrease to values near 0.94 for the Paschen series lines but produces ratio values near 1.05 for the longer wavelength series lines. There is also a profile mismatch for the $H\alpha$ line in order 2. The model also has a somewhat different shape around the series limits for the Paschen, Brackett, and Pfund series. The model falls below observations (including the Gaia DR3 prism spectrum) at wavelengths around 0.85, 1.47, and 2.2 μm leading to ratio values in the range 1.02 to 1.03. If the

corresponding Phoenix NewEra model is used in place of the Phoenix grid model the discrepancy in the region of the series limits is significantly worse. The Phoenix NewEra models are one-dimensional whereas the Husser et al. (2013) models use a spherical atmosphere model. It appears that a significant part of the discrepancy comes from geometrical effects in the stellar atmosphere model.

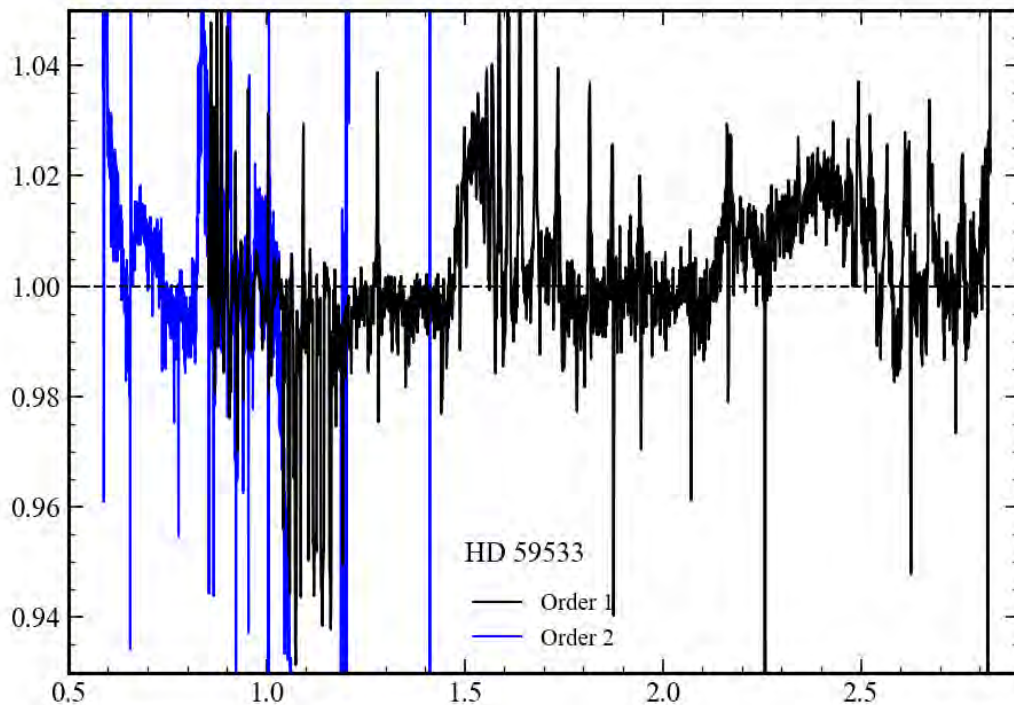


Figure 18: The ratio of the observed SOSS order 1 and order 2 spectra, after the correction of the photometric calibration with the weighted mean curves in Figure 16, and the Phoenix model.

For order 1 the ratio values are generally within 0.5% of 1 if the regions where the models have limitations are excluded. For order 2 the ratio values are between 0.99 and 1.02 for most of the wavelength range, increasing to about 1.05 right at the short wavelength end. The revision to the photometric calibration values combined with the background subtraction significantly improves the agreement between the stellar model prediction and the observed spectra.

9 Conclusions

All SOSS mode photometric observations taken from commissioning through the end of cycle 3 have been reduced and compared to model spectra for the stars from the CALSPEC web site. The background emission, primarily from the zodiacal light, affects all the observations but was not corrected for in the previous analysis because there was insufficient information about the background shape and its variability at different sky positions. In this analysis a background template shape created at the end of commissioning and 17 additional template shapes from the analysis of Baines et al. (2025) were used to match the individual background

Check with the JWST SOCCER Database at: <https://soccer.stsci.edu>

To verify that this is the current version.

shapes for each observation. In some of the cycle 3 observations a dedicated background observation was attached to the photometric observation and was available for the background subtraction. The spectra in SOSS orders 1 and 2 from the pipeline were averaged over the individual exposures of each observation, and then the ratio of these spectra to the CALSPEC models for the targets was determined. Some of the standard star observations are affected by contamination from either zero-order or first order spectra from other sources in the field.

The individual ratio functions were fit with smooth polynomial functions, or cubic spline fits where the shape was not well approximated by a polynomial function (usually due to sharp changes in the slope of the ratio function), and then these functions were combined to make mean ratio values. The averaging was carried out in two ways: first, a clipped mean with threshold of 3σ for order 1 and 2σ for order 2, which would be appropriate if the variation between the curves is to systematic errors from the background subtraction or the stellar models; and second, a weighted mean using the square-root of the total exposure time, which would be appropriate if the variation is entirely statistical. For order 2 the spectra become very faint for wavelengths greater than $1\ \mu\text{m}$, and there also appears to be difficulties in the spectral extraction at these wavelengths because of the overlap with order 1 on the detector. For the longer wavelength part of order 2 a fit to the higher S/N observation of BD+60°1753 was used in place of the mean values from all the standards. The weighted mean and clipped mean ratio functions differ by up to 2% level for order 1 and for the part of order 2 where the S/N is the highest, although for the regions of peak signal in order 1 the differences are less than 0.5%.

A test of the new photometric conversion factors was made using a calibration observation of the A-type star HD 59533. The JWST pipeline spectra for this star were corrected by the weighted mean ratio values derived from the photometric observations. A suitable stellar model was selected from the Phoenix model grid of Husser et al. (2013). Using the available photometry and the Gaia prism spectrum for this star the model was reddened to match the data. Comparison of the model and the SOSS observations shows some issues with the model at the various hydrogen series limits from 0.8 to $3\ \mu\text{m}$, but otherwise $\sim 0.5\%$ agreement is obtained for order 1 outside of the hydrogen absorption lines. For order 2 the agreement is at the $\pm 1\text{-}2\%$ level for the wavelengths where the S/N is high.

10 References

- Albert, L., Lafrenière, D., Doyon, R., et al., 2023, PASP, 135, 5001A.
- Baines, T., Carter, A., Espinoza, N., et al., 2025, Technical Report JWST-STScI-009046.
- Bohlin, R. C., Gordon, K. D., and Tremblay, P. E., 2014, PASP, 126, 711.
- Bohlin, R. C., Krick, J. E., Gordon, K. D., and Hubeny, I., 2022, AJ, 164, 10B.
- Bushouse, H., Eisenhamer, J., Dencheva, N., et al., 2025, JWST Calibration Pipeline 1.18.0, Zenodo, doi: 10.5281/zenodo.7038885.

Darveau-Bernier, A., Albert, L., Talens, G. J., et al., 2022, APSP, 134, 134:094502.

Gaia Collaboration, Prusti, T., de Bruijne, J. H. J., 2013, A&A, 595, A1.

Gaia Collaboration, Vallenari, A., Brown, A. G. A., et al., 2023, A&A, 674, A1.

Goodfrooij, P., Grumm, D., and Volk, K., 2024, PASP, 136, 4503G.

Husser, T.-O., Wende-von Berg, S., Dreizler, S., et al., 2013, A&A, 553, A6.

Ochsenbien, F., Bauer, P., and Marcout, J., 2000, A&AS, 143, 23.

Rieke, G., and Lebofsky, M. J., 1985, ApJ, 288, 618.

Volk, K., and the NIRISS Team, 2022, Technical Report JWST-STScI-008270.

Volk, K., 2024, Technical Report JWST-STScI-008778.

11 Appendix: Observation Log

The Table below lists the observations that were used in determining the photometric calibration values for the SOSS mode.

Table 3: The log of the NIRISS SOSS photometric calibration and photometric stability observations that were used in the analysis of the photometric calibration. Programs 1539, 4499, and 6607 are the photometric stability programs for cycles 1, 2, and 3 respectively. The other programs are the regular photometric calibration programs.

Program	Observation	Target	Date
1091	2	BD+60°1753	5 June 2022
1539	2	BD+60°1753	19 July 2022
1536	9	2MASS J17430448+6655015	9 August 2022
1539	77	BD+60°1753	30 August 2022
1539	27	BD+60°1753	16 September 2022
1537	2	G191 B2B	21 September 2022
1539	37	BD+60°1753	9 February 2023
1539	167	BD+60°1753	21 February 2023
1539	42	BD+60°1753	10 March 2023
1538	12	GSPC P177-D	2 April 2023
1539	47	BD+60°1753	6 April 2023
1539	52	BD+60°1753	3 May 2023
1539	57	BD+60°1753	30 May 2023
1539	62	BD+60°1753	30 June 2023
4499	4	BD+60°1753	6 July 2023
4499	11	BD+60°1753	30 July 2023

Check with the JWST SOCCER Database at: <https://soccer.stsci.edu>
To verify that this is the current version.

4498	24	GSPC P330-E	21 August 2023
4499	18	BD+60°1753	5 September 2023
4499	25	BD+60°1753	26 September 2023
4499	32	BD+60°1753	10 January 2024
4499	39	BD+60°1753	7 February 2024
4499	46	BD+60°1753	3 March 2024
4499	53	BD+60°1753	31 March 2024
4499	60	BD+60°1753	28 April 2024
4499	67	BD+60°1753	26 May 2024
4499	74	BD+60°1753	23 June 2024
6607	5	BD+60°1753	26 July 2024
6606	24	GSPC P330-E	5 August 2024
6607	115	BD+60°1753	25 September 2024
6607	112	BD+60°1753	8 January 2025
6607	114	BD+60°1753	1 April 2025
6607	113	BD+60°1753	2 May 2025
6606	42	GSPC P330-E	22 May 2025

Check with the JWST SOCCER Database at: <https://soccer.stsci.edu>
To verify that this is the current version.